ACS Photonics

Article

pubs.acs.org/journal/apchd5

Printable Surface Holograms via Laser Ablation

Fernando da Cruz Vasconcellos,*[,†,§] Ali K. Yetisen,[†,§] Yunuen Montelongo,[‡,§] Haider Butt,[‡,⊥] Alexandra Grigore,[†] Colin A. B. Davidson,[†] Jeff Blyth,[†] Michael J. Monteiro,[†,∥] Timothy D. Wilkinson,[‡] and Christopher R. Lowe*[,†]

[†]Department of Chemical Engineering and Biotechnology, University of Cambridge, Tennis Court Road, Cambridge CB2 1QT, U.K.

[‡]Centre for Advanced Photonics and Electronics, Department of Engineering, University of Cambridge, Cambridge CB3 0FA, U.K.

Supporting Information

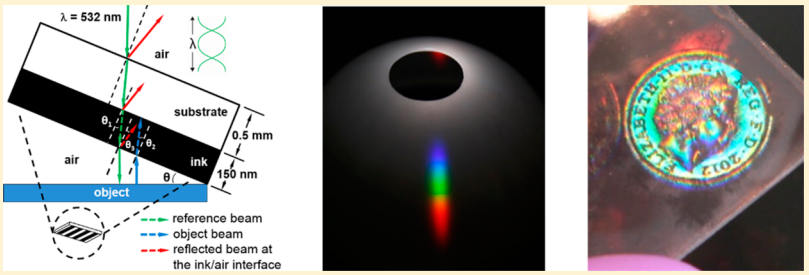

ABSTRACT: Holographic displays are used for applications in data storage, light trapping, security, sensing, and optical devices. Currently available fabrication techniques for holography remain expertise-dependent, costly, and time-consuming, limiting the widespread personalized use of holograms. The development of efficient and low-cost techniques for the rapid fabrication of holograms is required for practical applications. In this report, we use a single 6 ns laser pulse to record holographic surface gratings by ablation in well-ordered printed ink on a substrate. The entire hologram fabrication process can be completed within a few minutes. The photonic features of the prepared holograms have been modeled computationally and characterized experimentally. We demonstrate the versatility of our fabrication method by preparing 2D and 3D holograms on both optically transmissive and opaque surfaces. We anticipate that our strategy to fabricate holograms through laser ablation may hold great potential in personalized data storage, optical, and security applications.

KEYWORDS: *holography, laser ablation, diffraction gratings, printing, photonic devices*

Holograms in the visible and near-infrared region offer great promise in spectroscopic, light-trapping, optical filtering, laser tuning, security, display, and data storage applications.[1−3] A hologram is an optical element that can reconstruct a wavefront by means of diffraction. They are based on the spatial organization of static or dynamic diffraction fringes that disrupt the electromagnetic field, leading to changes in its intensity and/or phase. Traditional holograms are produced by the interference of coherent light.[4−6] Other methods include surface stamping/imprinting (i.e., embossing),[6] photochemical and electric field orientation of fringe elements,[7−9] and other more complex methods such as electron beam lithography (EBL)[10,11] and focused ion beam (FIB) milling.[12] Photochemical and electric-field-oriented gratings often require continuous external stimuli during operation, while the fabrication of EBL and FIB gratings is labor intensive, low-throughput, and costly. For practical applications, multibeam interference and surface stamping are currently the mostly widely used methods for the production of holograms since they are portable and require minimal or no external power for operation. However, the rapid fabrication of low-cost holograms on any flexible, rigid, or curved surface or material type for widespread personalized use remains a challenge.

Herein, we present a facile, low-cost, one-step process to fabricate well-ordered surface diffraction gratings and arbitrary holograms via a single collimated laser-light pulse over a coated surface. Patterning via laser ablation is a physical method to selectively remove light-absorbing material from localized regions.[13] The laser ablation method is fundamentally distinct from traditional patterning techniques, which require photochemical processing. In order to create well-localized ablated patterns, a short and high-intensity laser pulse is required.[14] The location precision of the ablation is governed by thermal diffusion in the light-absorbing material, which is directly related to the laser pulse intensity and duration.[15] Limiting thermal diffusion within the material is desirable for high-resolution patterning. Therefore, when a coherent light source creates a standing wave interference with sufficient localized energy, an ablated pattern with feature sizes comparable to the wavelength of the light can be formed. The energy absorbed by the light-absorbing material (i.e., ink-, pigment-, or dye-containing polymer resin) depends on the laser wavelength, energy, pulse duration, and the light absorbance properties of

Received: December 3, 2013
Published: April 8, 2014

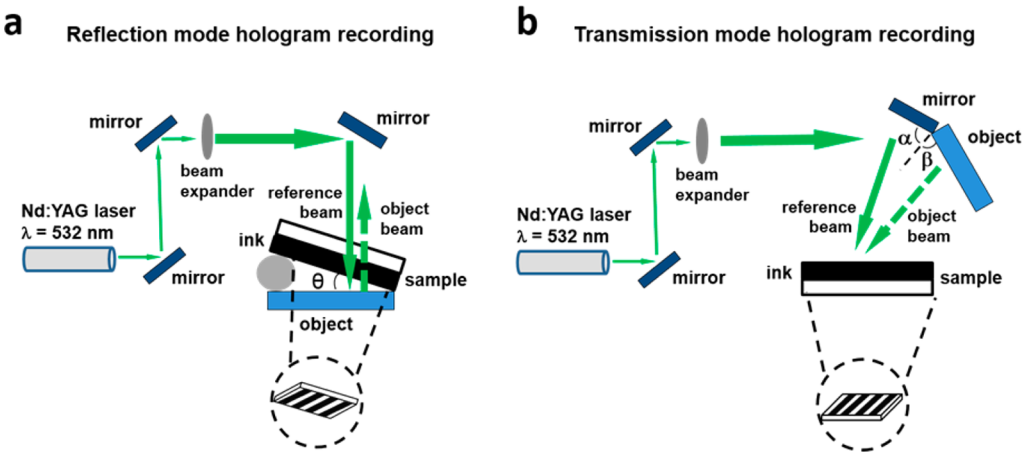

Figure 1. Surface hologram recording setups in reflection and transmission modes. Nd:YAG pulsed laser (λ = 532 nm) beam deviates from two mirrors and travels through a beam expander and (a) reflects off a third mirror before ablating the ink on the surface of a tilted (θ) substrate, backed by an object, or (b) reflects off a tilted mirror (α) and an object (β) simultaneously, resulting in two incident laser beams that interfere and ablate the ink on the surface of the substrate. All mirrors used were dielectric mirrors. Both reflection and transmission hologram recording modes had a laser beam spot size with a diameter ($\varnothing$) of ~1 cm.

the ablated material.[16] Laser ablation results in localized heat throughout the thin layer of the light-absorbing material, which undergoes photothermal evaporation and ejection from the surface.[17] The laser ablation process can also be employed to produce well-ordered surface diffraction gratings and holograms. These photonic structures can be prepared with complex geometries on various substrate types and surfaces, enabling high-throughput capability for an entire new range of optical applications.

We used nanosecond pulsed laser (λ = 532 nm) standing waves to ablate and produce patterned ink holographic diffraction gratings. Briefly, permanent black ink, consisting of blue, red, and yellow hues, was deposited on the surface of a flexible plastic substrate by mechanical writing (printing) or spin coating. Surface holograms were subsequently formed via a single 6 ns (~10 mJ) Nd:YAG laser pulse (Q-switch delay: 400 μs; spot size: 1 cm in diameter ($\varnothing$) after the beam expander) directed at the sample. We prepared surface holograms through two different recording setups: reflection[18] and transmission modes[6] (Figure 1). In the reflection holography recording setup, the laser beam was directed at the sample tilted at various angles (θ = 5−30°) from the normal, backed by a reflecting object (e.g., mirror or coin) normal to the laser incidence beam (Figure 1a). Here, the interference occurred between beams traveling in opposite directions. In the transmission recording setup (Figure 1b), the holographic surface grating was formed by the interference of two coherent incident beams, one reflected from a mirror and the other reflected off an object, directed at the sample, but at different angles (α and β). In both setups, the interference pattern of the wave fronts within the thin ink layer produced a well-ordered diffraction grating that diffracts light incident on the ink surface.

We modeled our system during hologram preparation using the superposition of different light waves in order to predict the interference pattern produced from the holographic surface grating. In the example of the in-line reflection hologram recording setup, we evaluated the interference pattern formed by three waves: (1) incident beam (reference beam), (2) beam reflected from the object (object beam), and (3) beam reflected internally at the ink/air interface (Figure 2a). In order to simplify the problem, only the s-polarized light (transverse electric (TE) mode waves) was analyzed. In the case of TE waves, the electric field vector of multiple waves points in the same direction. Therefore, there is only a single component of the electric vector $E(\mathbf{r},t)$ for all the waves. These components for the three planar waves can be defined as

$$E_1(\mathbf{r}, t) = A_1 e^{i(2\pi N(\mathbf{K_1}\cdot\mathbf{r})-\omega t+\phi_1)} \quad (1)$$

$$E_2(\mathbf{r}, t) = A_2 e^{i(2\pi N(\mathbf{K_2}\cdot\mathbf{r})-\omega t+\phi_2)} \quad (2)$$

$$E_3(\mathbf{r}, t) = A_3 e^{i(2\pi N(\mathbf{K_3}\cdot\mathbf{r})-\omega t+\phi_3)} \quad (3)$$

where A is the wave amplitude, $\mathbf{K}$ is the wave vector, ω is the angular frequency, ϕ is the phase, and $N = n + ik$ represents the complex refractive index. In a two-dimensional system, where the angle of the K vector with the normal is equal to θ, the electric vector $E(r,t)$ for the waves can be expressed as

$$E_1(x, y, t) = A_1 e^{(-2\pi k/\lambda)(x\sin(\theta_1)+y\cos(\theta_1))} \times e^{i[2\pi n/\lambda(x\sin(\theta_1)+y\cos(\theta_1))-\omega t+\phi_1]} \quad (4)$$

$$E_2(x, y, t) = A_2 e^{(-2\pi k/\lambda)(x\sin(\theta_2)+y\cos(\theta_2))} \times e^{i[2\pi n/\lambda(x\sin(\theta_2)+y\cos(\theta_2))-\omega t+\phi_2]} \quad (5)$$

$$E_3(x, y, t) = A_3 e^{(-2\pi k/\lambda)(x\sin(\theta_3)+y\cos(\theta_3))} \times e^{i[2\pi n/\lambda(x\sin(\theta_3)+y\cos(\theta_3))-\omega t+\phi_3]} \quad (6)$$

The three waves constructively and destructively interfere in the recording medium (ink), subsequently producing an intensity pattern. The mean value of the normalized intensity distribution, I, can be determined from the following equation:

$$\langle I(x, y)\rangle = \int_0^t |E_1(x, y, t) + E_2(x, y, t) + E_3(x, y, t)|^2 dt \propto |E_1(x, y) + E_2(x, y) + E_3(x, y)|^2 \quad (7)$$

We simulated the interference of the three plane waves by reconstructing the intensity distribution of the field along the thickness of the light-absorbing material (ink layer). The resulting interference pattern was determined by iteratively calculating the respective intensities and phases of the resulting

dx.doi.org/10.1021/ph400149m | ACS Photonics 2014, 1, 489−495

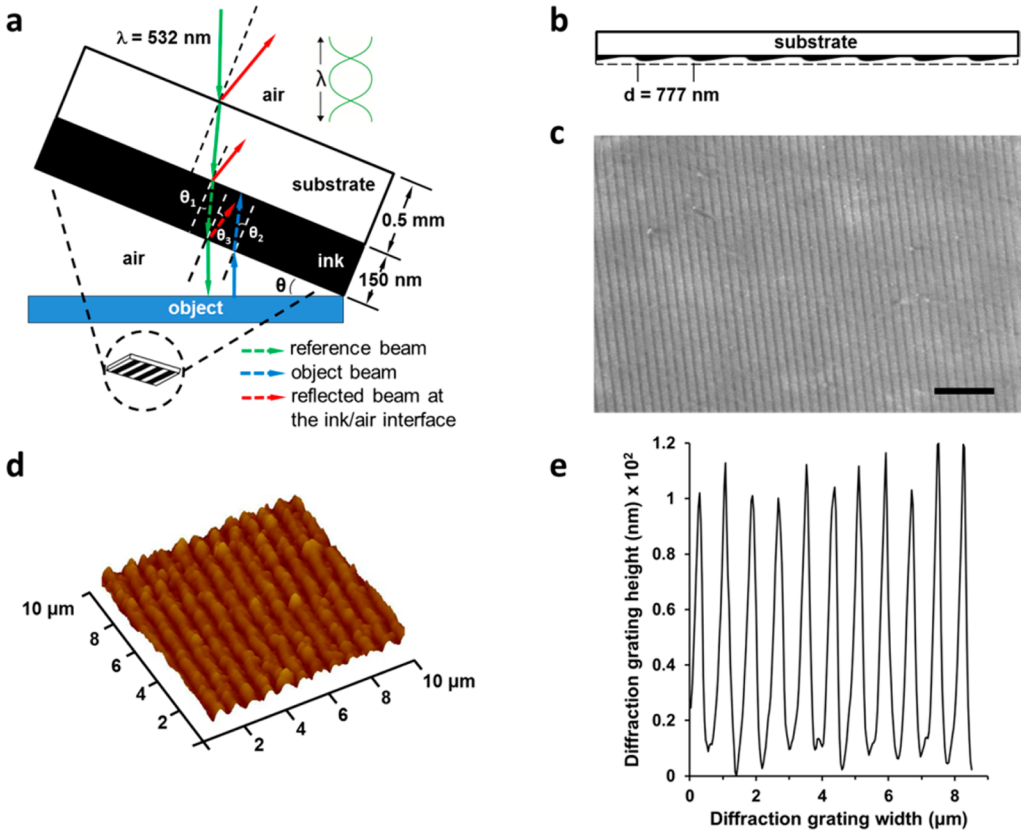

Figure 2. (a) Schematic representation of the interference pattern created from three waves, including (1) incident beam (reference beam), (2) beam reflected from the object (object beam), and (3) beam reflected internally at the ink–air interface. (b) Simulation of the interference of the three laser beams inside the ink layer resulting in the holographic surface grating, tilted at 20°. White regions within the dashed area represent ablated ink. (c) ESEM (scale bar 5 μm), (d) AFM, and (e) diffraction grating height (nm) of the surface holograms. Measured periodicity: ~750 nm.

wave. Using MATLAB, we visualized the intensity distribution in a 2D cross-sectional plane by evaluating the electromagnetic field at every point over a depth of 150 nm inside the ink layer. The interference pattern of the three distinct plane waves was determined by considering the laser wavelength, angle of incidence, refractive index, absorption (or extinction coefficient), and phase changes upon reflection (Figure 2b). The localization of heat along the standing wave was required to form a well-ordered surface diffraction grating structure. This requirement was achieved with short laser pulses (6 ns) of high intensity (~10 mJ) to minimize the diffusion of heat through the sample. The model was simplified by assuming that ablation occurs in specific locations in the material where the laser energy concentration exceeds a given threshold. A step function can be used to describe the ablated and nonablated regions along the surface of the material. By changing the threshold of the step function, different shapes in the oscillating diffraction patterns are formed. This is analogous to modifying the intensity of the laser light or changing the absorptive properties of the material. For instance, if the threshold is set to a low intensity, high volumes of the material are ablated; however low volumes of material are ablated when the threshold is defined at a high intensity.

The simulation in Figure 2b shows an ablation pattern produced by the interference of waves in the reflection mode recording setup in an optically transmissive substrate surface. In this case, the threshold was defined as half of the maximum normalized intensity. Holographic gratings were produced by the interference of waves. In the simulated pattern, black regions correspond to the non-ablated ink, while white regions represent ablated and removed ink from the surface. The resulting pattern corresponds to a skewed wave with a period of ~777 nm observed along the horizontal direction. The ablated material that is ejected in the vicinity of the sample may be removed with a suitable particulate vacuum extraction arm system.

Figure 2c shows an environmental scanning electron microscopy (ESEM) image of a surface hologram made from Staedtler Lumocolor permanent black ink, after laser ablation at θ = 20°. The periodicity was around 750 nm, which is in good agreement with the theoretically calculated grating spacing of 777 nm. The difference between the two may be attributed to the mechanical simplicity of the optical setup and measurement errors in accurately determining the ink layer thickness, inclined angle of the substrate, and angle of incident laser beams. This spacing was further supported by topographic characterization using atomic force microscopy, giving an average surface grating depth of ~117 nm (Figure 2d,e).

Experimentally, the surface diffraction grating showed broadband diffraction. Using COMSOL Multiphysics, we simulated the optical diffraction using the finite element method (Figure 3). By directing incident light of three different wavelengths (445, 532, and 650 nm; blue, green, red) at the ink-based surface gratings, we evaluated the resulting diffraction patterns. Figure 3a shows the geometry of the simulated model where the diffraction grating was illuminated at a normal incidence. The grating dimensions were set according to the AFM measurements. A hemispherical model geometry (⌀ 32

dx.doi.org/10.1021/ph400149m | ACS Photonics 2014, 1, 489–495

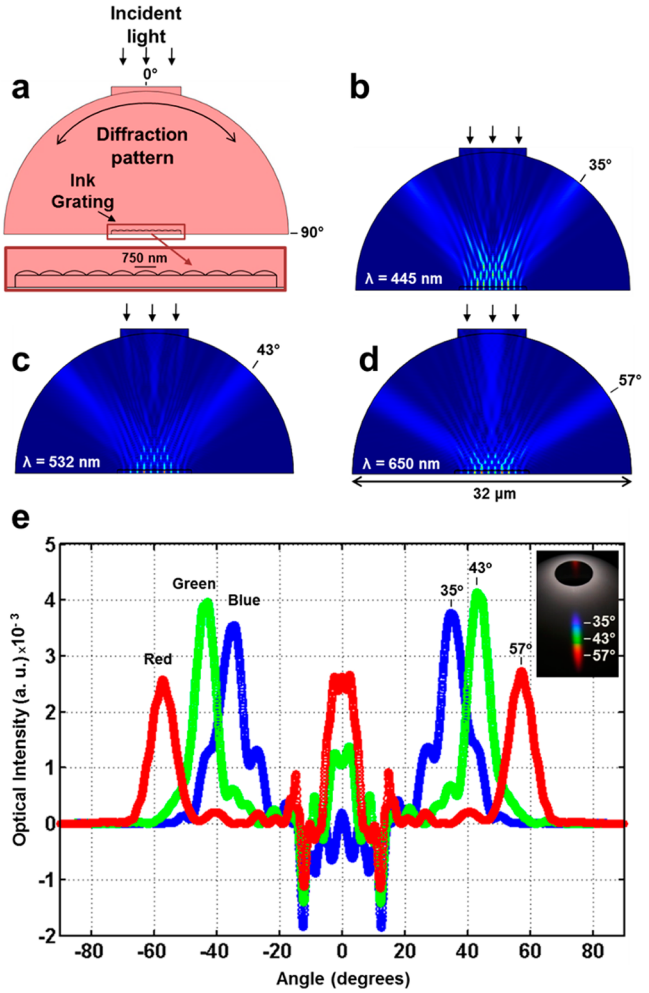

Figure 3. (a) COMSOL Multiphysics simulation model geometry with the inset showing the dimensions of the grating. The diffraction patterns were simulated in response to (b) blue (445 nm), (c) green (532 nm), and (d) red (650 nm) wavelengths. Diffraction patterns range from low (i.e., dark blue) to higher (i.e., light blue) optical intensities. (e) Optical intensity plots as a function of angle across the hemispherical boundary. The experimental diffraction of a sample (ablated at $\theta = 20°$) for the complete optical spectra is shown in the inset.

μm) was chosen to simulate the diffraction pattern generated by the surface grating, which was defined using a plastic substrate in air.

Figure 3b–d show the simulated diffraction produced in response to blue (445 nm), green (532 nm), and red (650 nm) wavelengths. The diffraction angle increased with the increase in wavelength. Far-field optical intensity across the hemispherical boundary was also plotted as shown in Figure 3e. The intensity plots for each wavelength showed the interference pattern produced from −90 to +90 degrees. At larger angles, symmetrical higher orders were observed. The diffraction angles increased with the increase in wavelength. The simulations also predicted that the diffraction efficiency decreased with the increase in wavelength.

Theoretically, grating periods of 3052, 1532, 1028, and 777 nm can be obtained by ablating samples at tilt angle of 5°, 10°, 15°, and 20°, respectively. The grating periods can be calculated by projecting the standing wave over the tilt angle of the sample. In order to determine the period of the grating formed by the main standing waves, we considered the reference and object electric fields. Propagation of both waves inside the medium have opposite direction ($\mathbf{K} = \mathbf{K}_1 = -\mathbf{K}_2$ and $\theta = \theta_1 = \theta_2 + 180$) and a phase difference between them (ϕ) is given by

$$\begin{aligned}\langle I(x, y)\rangle &\propto |E_1(x, y) + E_2(x, y)|^2 \\ &= |e^{i(2\pi N(\mathbf{K}\cdot\mathbf{r}))} + e^{i(-2\pi N(\mathbf{K}\cdot\mathbf{r})+\phi)}|^2 \\ &= 1 + \cos\left(2\pi\frac{2N}{\lambda}(x\sin(\theta) + y\cos(\theta)) + \phi\right)\end{aligned} \tag{8}$$

Considering the real part of N, the period of the grating (λ_g) at a constant position y can be expressed as

$$\langle I(x)\rangle \propto 1 + \cos\left(2\pi\frac{x}{\lambda_g} + \phi\right),\ \lambda_g = \frac{\lambda}{2\sin(\theta)} \tag{9}$$

where θ is the tilt angle of the sample.

Experimental data of the diffraction spectra for samples ablated at these angles showed that the diffraction efficiency increased for large tilt θ angles (Figure 4). The diffraction efficiency was maximized when the length of the period of the surface grating was close to the wavelength of the incident light. For periods on the order of 777 nm, the grating produced only first-order diffraction, and hence an increased efficiency was observed. The diffraction pattern consists of spots for each color of light, with red diffracted at higher angles and blue at lower angles, in agreement with theory (Figure 3b–d). If the diffraction grating is illuminated with a laser, two spots are diffracted in the backward direction and two spots in the forward direction (see Supporting Information). For example, the hologram prepared at a tilt angle of 20° was illuminated with a 650 nm laser, and its diffraction efficiency was determined by adding these four diffracted spots with an optical power meter. The maximum diffraction efficiency was measured to be 12% by adding the two transmissive and the two reflective spots. From this scattered light, ~40% contributes to the reflective diffraction (~20% and ~20% for

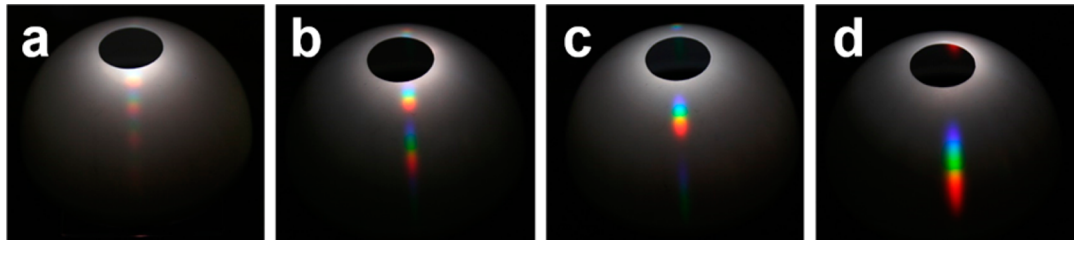

Figure 4. Diffraction patterns produced by the ink gratings in response to incident light. Camera images for the diffraction responses for gratings produced by laser ablation at tilt θ angles of (a) 5°, (b) 10°, (c) 15°, and (d) 20°.

dx.doi.org/10.1021/ph400149m | ACS Photonics 2014, 1, 489–495

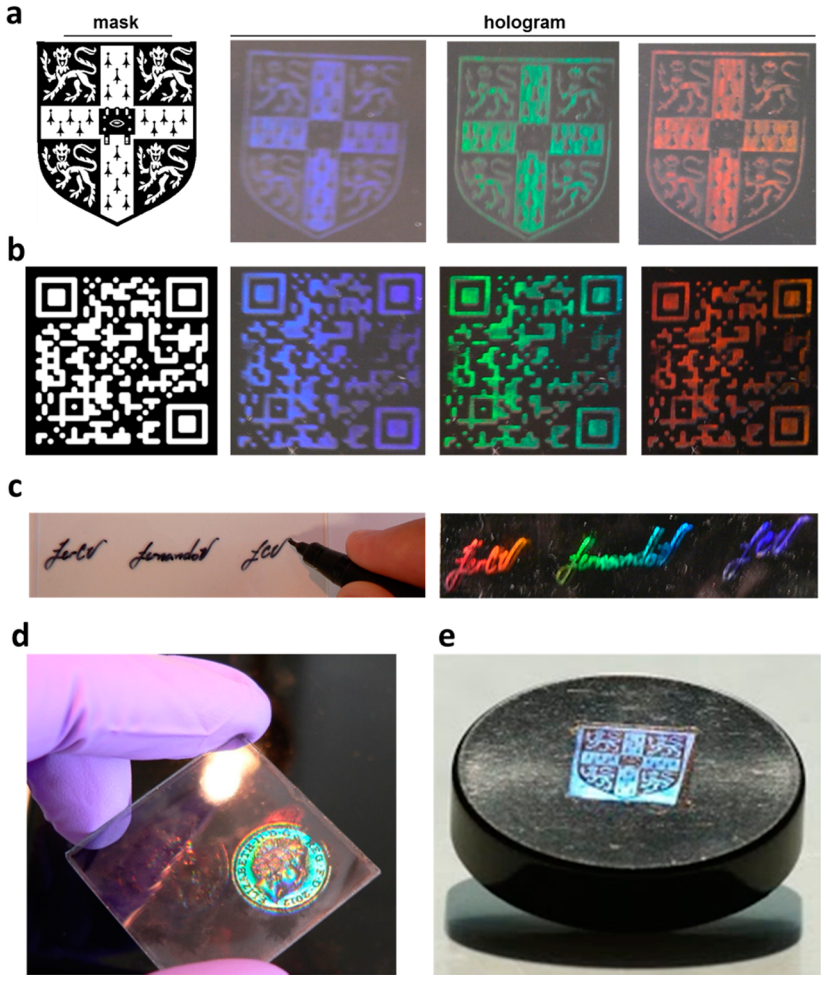

Figure 5. Fabrication of surface holograms via printing and laser ablation. Images show different replay diffractions of the surface holograms as a function of incident light angle. Holographic (a) logo, (b) QR code, (c) signature, (d) 3D coin (full parallax) on a transparent surface, and (e) image on an opaque black surface.

each spot) and ~60% to the transmissive diffraction (~30% and ~30% for each spot).

We used five examples to demonstrate the utility of surface holograms produced with this new method. In the first example, an image was printed on a transparency (Figure 5a). This transparency was used as a mask to selectively ablate areas over an ink spin-coated poly(methyl methacrylate) (PMMA) substrate. The logo can be printed directly, for example, by inkjet printing or stamping, and ablated to achieve a surface hologram. The resulting pattern acts as a surface grating, and the diffraction was visible to the naked eye. We next demonstrated a hologram on a printed QR code that could be used for security identification applications (Figure 5b). The end user can decode it using a smartphone, and the verification can be based on pass/fail and will thus enhance the authentication of the product. In the next example, we demonstrated a handwritten holographic signature (Figure 5c). The signature was written on a pressure-sensitive tape and ablated to produce the hologram. Such holographic signatures may be used in personalizing and authenticating autographs. Figure 5d illustrates a three-dimensional (3D) hologram using a coin as the object in Figure 1a. The observed image exhibits 3D full parallax when viewed from different angles, as well as a change in the diffraction wavelength.

The methodology of recording holograms in reflection mode allows the fabrication of a wide range of holograms on substrates that are transparent. This provides the advantage that the holograms are visible from both sides of the substrate. When the holograms are viewed from the backside of the substrate, they appear as the pseudoscopic images of the holograms when viewed from the frontside of the substrate. We can prepare the same surface diffraction patterns through a transmission recording mode (Figure 1b). This alternative recording mode allows the recording of holograms on opaque surfaces where the reflection mode recording is not possible. The final example (Figure 5e) shows a surface hologram prepared on an opaque surface (i.e., bottle cap of a chemical reagent) by transmission mode holographic recording using a mask. These examples demonstrate the potential of the laser ablation technique for preparing holograms on both transparent and opaque materials.

CONCLUSION

We developed a simple and low-cost holographic recording method to fabricate surface diffraction gratings via printing and single-step pulsed laser ablation. Our strategy has many attractive attributes due to its exceptionally simple setup and flexibility. It allows the use of a diverse array of materials as substrates, including transparent and opaque polymers and

dx.doi.org/10.1021/ph400149m | ACS Photonics 2014, 1, 489−495

silicon-based and ceramic materials, with simple or complex geometries. Other laser light absorbing inks, dyes, nanoparticles, metals, and biomolecules can also be used to achieve well-ordered surface holograms with this method. We demonstrated the utility of our technique using various printed patterns and their applications. Our fabrication technique is scalable for printing low-cost holograms. The light-absorbing material can be printed on a substrate using various methods, including inkjet printing, spin coating, stamping, or screen-printing, followed by laser ablation within minutes. Additionally, computational simulations can predict the photonic characteristics of the holograms and therefore their applications. Our surface holograms may find numerous novel applications in secure data storage, personalized artwork, identification (business cards), sensing, and security. We envision that our technology can be integrated in desktop printers for easy-to-fabricate holograms from data storage to optical displays and devices.

MATERIALS AND METHODS

Lumocolor permanent black ink was supplied from Staedtler (Nuremberg, Germany). Poly(methyl methacrylate) (0.5 mm thick) was purchased from Goodfellow Cambridge Ltd. (Huntingdon, U.K.). Nd-yttrium-aluminum-garnet pulsed laser (high-power compact Q-switched Nd:YAG oscillator with super Gaussian resonator, 700 mJ @ 1064 nm, 10 Hz) with a second-harmonic generator (6 ns, 350 mJ @ 532 nm, 10 Hz, thermally stabilized with wavelength separation) was purchased from Lambda Photometrics (Harpenden, U.K.). The ink was characterized using UV-vis spectroscopy (DU 800, Beckman Coulter) (see Supporting Information).

Preparation of Surface Gratings. Holographic surface diffraction gratings were prepared by creating well-ordered ink structures on various substrates via laser ablation. First, substrates were coated with ink. The ink thickness (~150 nm, measured with profilometry) was controlled using spin coating. Well-ordered ink structures were formed with two different hologram recording setups. In the first setup (in-line reflection), holograms were prepared via a single 6 ns pulse of laser beam directed at the sample elevated at various angles (0–30°) from the normal, backed by an object. In the second recording setup (transmission mode), the interference of two coherent laser beams, directed at the sample from the same direction, was used to prepare the surface holograms.

ASSOCIATED CONTENT

Supporting Information

Includes details on UV characterization of the ink, spin coating of ink over substrates, mask preparation, and instruments and methods used in the characterization of printable surface holograms via laser ablation. This material is available free of charge via the Internet at http://pubs.acs.org.

AUTHOR INFORMATION

Corresponding Authors

*E-mail: (F. C. Vasconcellos) fcv21@cam.ac.uk.
*E-mail: (C. R. Lowe) crl1@cam.ac.uk.

Present Addresses

[‖]Australian Institute for Bioengineering and Nanotechnology, University of Queensland, Brisbane 4072, Australia.
[⊥]School of Mechanical Engineering, University of Birmingham, Edgbaston, Birmingham B15 2TT, UK.

Author Contributions

[§]F. C. Vasconcellos, A. K. Yetisen, and Y. Montelongo contributed equally.

Notes

The authors declare no competing financial interest.

ACKNOWLEDGMENTS

The authors thank Jon Rickard, from the Cavendish Laboratory, for ESEM sample preparation. Y.M. thanks CONACYT for financial support. F.C.V. gratefully thanks Prof. Elza da Costa Cruz Vasconcellos, from UNICAMP, for fruitful discussions and the Post-Doctoral Fellowships from FAPESP, Grant No. 2011/06906-6 and CNPq INCTBio, Grant No. 209869/2013-5.

REFERENCES

(1) Tay, S.; Blanche, P. A.; Voorakaranam, R.; Tunç, A. V.; Lin, W.; Rokutanda, S.; Gu, T.; Flores, D.; Wang, P.; Li, G.; St Hilaire, P.; Thomas, J.; Norwood, R. A.; Yamamoto, M.; Peyghambarian, N. An updatable holographic three-dimensional display. *Nature* **2008**, *451*, 694–698.

(2) Blanche, P. A.; Bablumian, A.; Voorakaranam, R.; Christenson, C.; Lin, W.; Gu, T.; Flores, D.; Wang, P.; Hsieh, W. Y.; Kathaperumal, M.; Rachwal, B.; Siddiqui, O.; Thomas, J.; Norwood, R. A.; Yamamoto, M.; Peyghambarian, N. Holographic three-dimensional telepresence using large-area photorefractive polymer. *Nature* **2010**, *468*, 80–83.

(3) Smalley, D. E.; Smithwick, Q. Y. J.; Bove, V. M.; Barabas, J.; Jolly, S. Anisotropic leaky-mode modulator for holographic video displays. *Nature* **2013**, *498*, 313–317.

(4) Jang, J. H.; Ullal, C. K.; Maldovan, M.; Gorishnyy, T.; Kooi, S.; Koh, C. Y.; Thomas, E. L. 3D micro- and nanostructures via interference lithography. *Adv. Funct. Mater.* **2007**, *17*, 3027–3041.

(5) Xia, D.; Ku, Z.; Lee, S. C.; Brueck, S. R. Nanostructures and functional materials fabricated by interferometric lithography. *Adv. Mater.* **2011**, *23*, 147–179.

(6) Saxby, G. *Practical Holography*, 3rd ed.; Institute of Physics Publishing: UK, 2004.

(7) Ikeda, T. Photomodulation of liquid crystal orientations for photonic applications. *J. Mater. Chem.* **2003**, *13*, 2037–2057.

(8) Llordes, A.; Garcia, G.; Gazquez, J.; Milliron, D. J. Tunable near-infrared and visible-light transmittance in nanocrystal-in-glass composites. *Nature* **2013**, *500*, 323–326.

(9) Sasaki, T.; Ikegami, M.; Abe, T.; Miyazaki, D.; Kajikawa, S.; Naka, Y. Real-time dynamic hologram in photorefractive ferroelectric liquid crystal with two-beam coupling gain coefficient of over 800 cm^{-1} and response time of 8 ms. *Appl. Phys. Lett.* **2013**, *102*, 063306–063306–4.

(10) Butt, H.; Montelongo, Y.; Butler, T.; Rajesekharan, R.; Dai, Q.; Shiva-Reddy, S. G.; Wilkinson, T. D.; Amaratunga, G. A. J. Carbon nanotube based high resolution holograms. *Adv. Mater.* **2012**, *24*, OP331–OP336.

(11) Montelongo, Y.; Tenorio-Pearl, J. O.; Milne, W. I.; Wilkinson, T. Polarization switchable diffraction based on subwavelength plasmonic nanoantennas. *Nano Lett.* **2014**, *14*, 294–298.

(12) Marshall, O. P.; Chakraborty, S.; Khairuzzaman, M.; Beere, H. E.; Ritchie, D. A. Reversible mode switching in Y-coupled terahertz lasers. *Appl. Phys. Lett.* **2013**, *102*, 111105–111105–5.

(13) Plech, A.; V, K.; Lorenc, M.; Boneberg, J. Femtosecond laser near-field ablation from gold nanoparticles. *Nat. Phys.* **2006**, *2*, 44–47.

(14) Chung, J.; Han, S.; Lee, D.; Ahn, S.; Grigoropoulos, C. P.; Moon, J.; Ko, S. H. Nanosecond laser ablation of silver nanoparticle film. *Opt. Eng.* **2013**, *52*, 24302–24302.

(15) Semaltianos, N. G. Nanoparticles by Laser Ablation. *Crit. Rev. Solid State* **2010**, *35*, 105–124.

(16) Leal-Ayala, D. R.; Allwood, J. M.; Counsell, T. A. M. Paper unprinting: using lasers to remove toner-print in order to reuse office paper. *Appl. Phys. A: Mater.* **2011**, *105*, 801–818.

(17) Leal-Ayala, D. R.; Allwood, J. M.; Schmidt, M.; Alexeev, I. Toner-print removal from paper by long and ultrashort pulsed lasers. *Proc. R. Soc. A* **2012**, *468*, 2272−2293.
(18) Benton, S. A.; Bove, V. M., *In-Line "Denisyuk" Reflection Holography*; John Wiley & Sons, Inc.: New York, 2007; pp 173−180.

NOTE ADDED AFTER ASAP PUBLICATION

Figure 2e was revised after this paper was published ASAP on April 8, 2014. The corrected version was reposted on April 10, 2014.